REPORT

An interphase contractile ring reshapes primordial germ cells to allow bulk cytoplasmic remodeling

Chelsea Maniscalco[1], Allison E. Hall[1], and Jeremy Nance[1,2]

Some cells discard undesired inherited components in bulk by forming large compartments that are subsequently eliminated. ***Caenorhabditis elegans*** **primordial germ cells (PGCs) jettison mitochondria and cytoplasm by forming a large lobe that is cannibalized by intestinal cells. Although PGCs are nonmitotic, we find that lobe formation is driven by constriction of a contractile ring and requires the RhoGEF ECT-2, a RhoA activator also essential for cytokinesis. Whereas centralspindlin activates ECT-2 to promote cytokinetic contractile ring formation, we show that the ECT-2 regulator NOP-1, but not centralspindlin, is essential for PGC lobe formation. We propose that lobe contractile ring formation is locally inhibited by the PGC nucleus, which migrates to one side of the cell before the cytokinetic ring assembles on the opposite cortex. Our findings reveal how components of the cytokinetic contractile ring are reemployed during interphase to create compartments used for cellular remodeling, and they reveal differences in the spatial cues that dictate where the contractile ring will form.**

Introduction

Developing and differentiating cells often inherit unneeded gene products or organelles. Such components can be eliminated individually, such as in the targeted degradation of transcription factors (Page et al., 2007), or via the autophagic removal of entire organelles (Sato and Sato, 2017). Alternatively, some cells discard contents in bulk by creating a compartment that is filled with undesired cellular material and eliminated. For example, during erythropoiesis in mammals, erythroblasts form a subcellular compartment containing the nucleus, which is subsequently removed and digested by macrophages to leave behind an anucleate immature red blood cell (Moras et al., 2017). Similar remodeling events occur in the germ line, such as during spermatogenesis, when many cellular components are discarded in the residual body (Nishimura and L'Hernault, 2017). We recently described a bulk remodeling event in *Caenorhabditis elegans* embryonic primordial germ cells (PGCs), which produce large lobes that are filled with mitochondria and other cellular components; subsequently, adjacent intestinal cells cannibalize the lobes, remodeling the PGCs and their contents (Abdu et al., 2016). In each of these examples, the discarded compartment forms through changes in cell shape involving localized constrictions at the cell surface (Abdu et al., 2016; Breucker et al., 1985; Koury et al., 1989). The cellular mechanisms used to create and eliminate such compartments are not well understood.

Forces driving constriction of the plasma membrane typically arise from the localized contraction of myosin on cortical microfilaments (Martin and Goldstein, 2014; Munjal and Lecuit, 2014). Cytokinesis is a well-studied example. During cytokinesis, a contractile ring enriched in myosin, F-actin, and cross-linking and anchoring proteins such as anillin and septin, enriches in a zone at the cell equator (Glotzer, 2017; Srivastava and Robinson, 2015). The contractile ring narrows in circumference, generating forces that cause the plasma membrane to ingress. Centralspindlin, a complex of the kinesin-6 MKLP1 and MgcRacGAP (Basant and Glotzer, 2018), accumulates at the spindle midzone and at the future site of furrow formation, where it activates a cortical pool of the RhoGEF Ect2. In turn, Ect2 locally activates RhoA, which activates myosin and the actin nucleator formin, leading to assembly and contraction of the contractile ring (Green et al., 2012). Contractile rings have also been described in a few types of nonmitotic cells, such as enucleating erythroblasts, ascidian notochord cells, and budding *Drosophila melanogaster* pole cells (Cinalli and Lehmann, 2013; Koury et al., 1989; Sehring et al., 2015). The cues responsible for forming and positioning contractile rings in nondividing cells are poorly understood. Here, we show that a nonmitotic contractile ring induces lobe formation in *C. elegans* PGCs, and we identify cellular and molecular pathways that induce its formation. Our findings provide a cell biological mechanism for

---

[1]Skirball Institute of Biomolecular Medicine, New York University School of Medicine, New York, NY; [2]Department of Cell Biology, New York University School of Medicine, New York, NY.

Correspondence to Jeremy Nance: jeremy.nance@med.nyu.edu.

forming transient compartments that are used to discard cellular content in bulk.

Results and discussion

A contractile ring assembles at the PGC lobe neck

The two *C. elegans* PGCs form lobes several hours after their birth (Abdu et al., 2016; Sulston et al., 1983). We visualized PGC lobe formation by acquiring movies of embryos expressing PGC-specific membrane-localized mCherry (Mem[PGC]; Video 1). Movies began before lobes formed (bean stage), when both PGCs were visible within a plane (Fig. 1 a). During the period of lobe formation (by comma stage), embryos rotated 90° such that only one PGC was visible (Fig. 1 a''). Just before lobes formed, PGCs transitioned from a nearly spherical to an elliptical shape with an increased aspect ratio (Fig. 1, a', b, and b'). Subsequently, PGCs constricted centrally to adopt an hourglass shape with a large lobe (L) on one side of the cell and the cell body containing the nucleus (*) on the other (Fig. 1 a''; see also Fig. 5 e). This transition occurred within an hour. Lobe cannibalism (not depicted) occurs at a later stage of embryogenesis (Abdu et al., 2016).

PGCs form lobes without changes to cell volume and when cultured in isolation, indicating that lobe formation is an autonomously driven cell shape change (Abdu et al., 2016). Although PGCs are arrested in G2 (Fukuyama et al., 2006), lobe formation resembles an incomplete cytokinesis. To determine if a contractile ring could provide the forces for lobe formation, we examined contractile ring components in PGCs as they formed lobes (Fig. 1 c). We first examined the myosin heavy chain NMY-2 using a functional *nmy-2-gfp* knockin (Dickinson et al., 2013) and a PGC-specific *nmy-2-yfp* transgene (NMY-2-YFP[PGC]). In addition to accumulating at the intercellular bridge that connects the two PGCs (the result of an incomplete cytokinesis; Goupil et al., 2017; Sulston et al., 1983), NMY-2-GFP and NMY-2-YFP[PGC] concentrated at the base of PGC lobe necks within a ring (Video 2), which when viewed in cross section appear as two foci (Fig. 1, e–e''', arrowheads). Both fusion proteins colocalized at the PGC lobe neck ring (Fig. 1, e''' and f), and puncta of NMY-2-YFP[PGC] appeared at incipient lobe necks as they first began to form (Fig. S1, a–a''). These observations suggest that myosin might provide forces that induce the PGC membrane to ingress.

Anillin is a contractile ring cross-linking protein that binds to F-actin, myosin, and septins (Piekny and Maddox, 2010). The anillin homologue ANI-1, like NMY-2, concentrated in a ring at the base of PGC lobes (Fig. 1, g–g''' and h). Septins are filamentous proteins that enrich in contractile rings (Mostowy and Cossart, 2012). *C. elegans* contains two septins, UNC-59 and UNC-61, whose products associate interdependently (Nguyen et al., 2000). UNC-59 and NMY-2 also coenriched at the base of lobe necks (Fig. 1, i–i''' and j). We examined PGC F-actin localization indirectly by expressing the actin-binding protein Moesin-GFP specifically in PGCs. Before PGC lobes formed, GFP-Moesin[PGC] was enriched uniformly at the cell cortex (Fig. 1 k'). After lobes formed, GFP-Moesin[PGC] was distributed throughout the cell cortex (Fig. 1, l–l' and m) and also accumulated within the

lobe, suggesting that F-actin may have an additional function within lobes. We conclude that a contractile ring enriched in myosin, anillin, and septin assembles at the PGC lobe neck.

Formin and myosin are required for PGC lobe formation

To determine whether contractile ring components are needed for lobe formation, we used temperature-sensitive alleles of genes required for cytokinesis. *cyk-1* encodes the *C. elegans* Diaphanous family formin (Mi-Mi et al., 2012), which promotes unbranched actin polymerization and is critical for cytokinesis (Bohnert et al., 2013; Davies et al., 2014). We upshifted synchronized *cyk-1* mutant embryos to the restrictive temperature just before lobes normally form, capturing an image stack at this time (t = 0 min) and nearly 2 h later (t = 108 min), when PGCs in WT embryos have formed lobes (Fig. 2 a; temperature-shift regime I). PGCs failed to form lobes in most *cyk-1* mutants (no lobes, Class I; Fig. 2, c' and f), in contrast to WT control embryos imaged on the same slide (Fig. 2, b' and f), suggesting that formin-mediated linear F-actin polymerization is required for lobe formation.

We next examined the requirement for myosin using the *nmy-2(ne3409ts)* temperature-sensitive allele, which contains a missense mutation within the S2 region (Liu et al., 2010) important for dimerization and motor activity (Tama et al., 2005). PGCs formed lobes in only 5% of *nmy-2* embryos (Fig. 2 g), and mutants fell into two phenotypic classes. In a small fraction of embryos, PGCs remained spherical and did not form lobes, similar to *cyk-1* mutant embryos (no lobes, Class I; Fig. 2, d' and g). The majority of *nmy-2* mutants showed an additional defect, forming a bubble-shaped expansion at the connection between the PGCs (no lobes, Class II; Fig. 2, e' and g), which we suspected was an expansion of the intercellular bridge connecting the PGCs. To test this hypothesis, we expressed the centralspindlin component ZEN-4, a marker of division remnants (Raich et al., 1998), specifically in PGCs. ZEN-4-YFP[PGC] accumulated at the division remnant between the PGCs in WT embryos (Fig. 2 h) but was not present at PGC lobe necks (Fig. 2 i). In most *nmy-2* embryos that were upshifted at a stage before lobes normally form (Fig. 2 j), a bubble developed between the two PGCs (17/22 embryos) that invariably contained a focus of ZEN-4-YFP[PGC] (17/17 embryos; Fig. 2, k–k''). These findings indicate that *nmy-2* is required both to maintain the PGC intercellular connection, as previously shown (Goupil et al., 2017), and to form lobes, suggesting that myosin-mediated contraction of F-actin in the contractile ring provides the forces that promote lobe neck ingression.

PGC lobe formation requires *ect-2*

In dividing cells, RhoA triggers contractile ring formation by activating formin (Otomo et al., 2005; Watanabe et al., 2008) and myosin (Kosako et al., 2000). Given that formin and myosin are required for lobe formation, we considered the RhoA homologue RHO-1 a likely activator of the lobe neck contractile ring. We examined the requirement for RHO-1 indirectly using a temperature-sensitive allele of its activator ECT-2 (Zonies et al., 2010), which localizes through the cortex of PGCs (Fig. 3, a and a'). 71% of the *ect-2* mutant embryos that

Maniscalco et al.
Primordial germ cell remodeling by a contractile ring

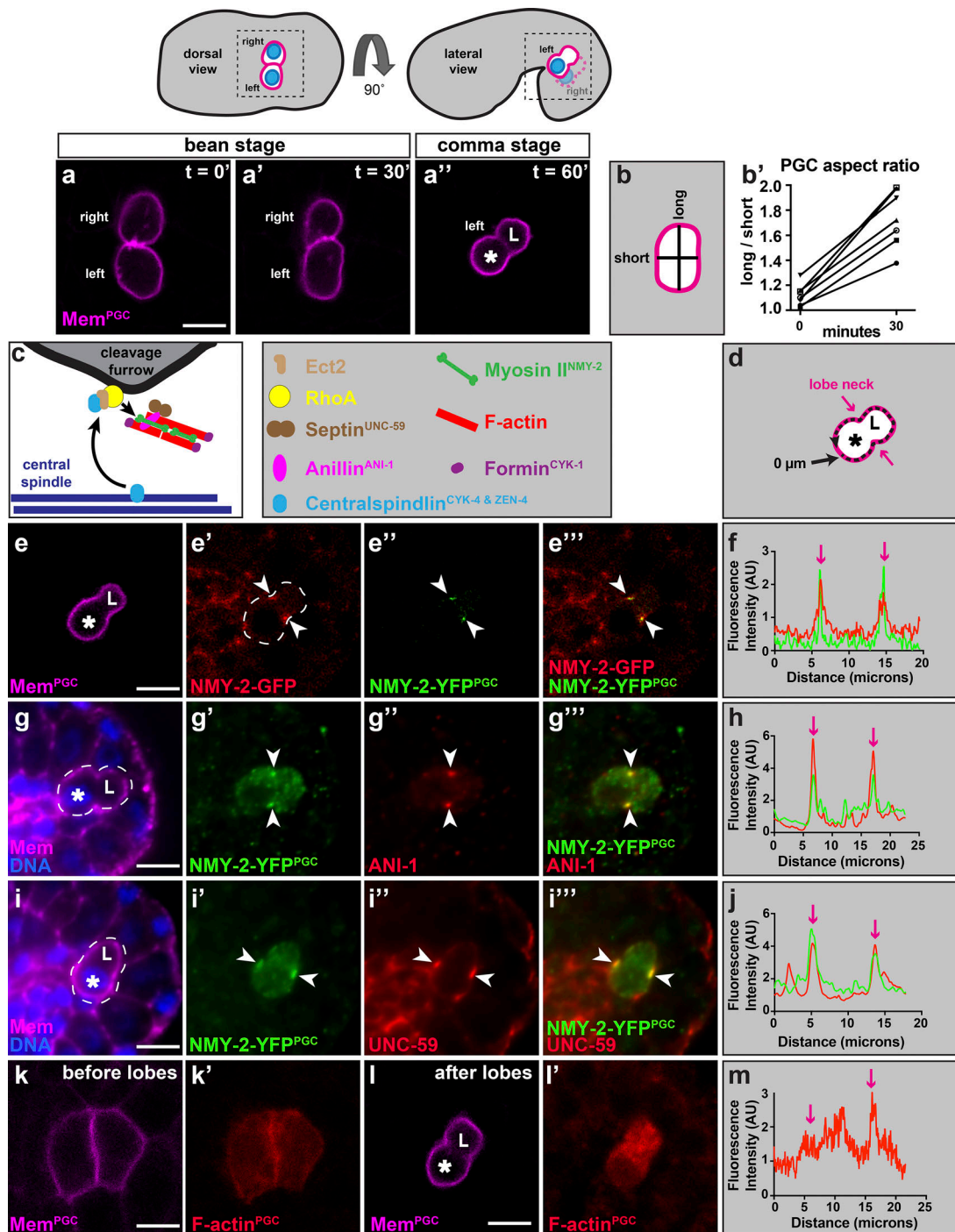Journal of Cell Biology
https://doi.org/10.1083/jcb.201906185

2

Figure 1. **A contractile ring forms at the PGC lobe neck. (a–a'')** Time-lapse stills showing steps of PGC lobe formation Top: Corresponding embryonic stages and orientations are shown (PGC nuclei are blue). **(b and b')** Aspect ratios of seven PGCs at the times corresponding to panels a and a'. **(c)** Cytokinetic furrow showing contractile ring components and regulators. **(d)** Schematic illustrating starting and ending points for cortical intensity traces. Pink arrows indicate lobe necks; dashed black line with arrowhead indicates starting and stopping points for traces. **(e–j)** Colocalization of the indicated proteins at the lobe contractile ring (arrowheads); pink arrows indicate lobe neck position in intensity traces. **(k–l')** F-actin detected with Moesin-GFP[PGC] before and after lobe formation. **(m)** Cortical intensity trace of F-actin[PGC] from the image shown in l'; pink arrows indicate lobe neck position. Dashed white line indicates outline of PGC, * indicates nuclear position, and L indicates the lobe. Scale bar, 5 μm.

were upshifted using temperature-shift regime I failed to form PGC lobes (Fig. 3, c–e). These included Class I embryos specifically defective in lobe formation (Fig. 3, c and c'); Class II embryos with an expanded intercellular bridge; and Class III embryos, which contained a binucleate PGC lacking lobes (Fig. 3, d and d'). The finding that ECT-2 is required for PGC lobe formation strongly suggests that active RHO-1 induces PGC lobe formation.
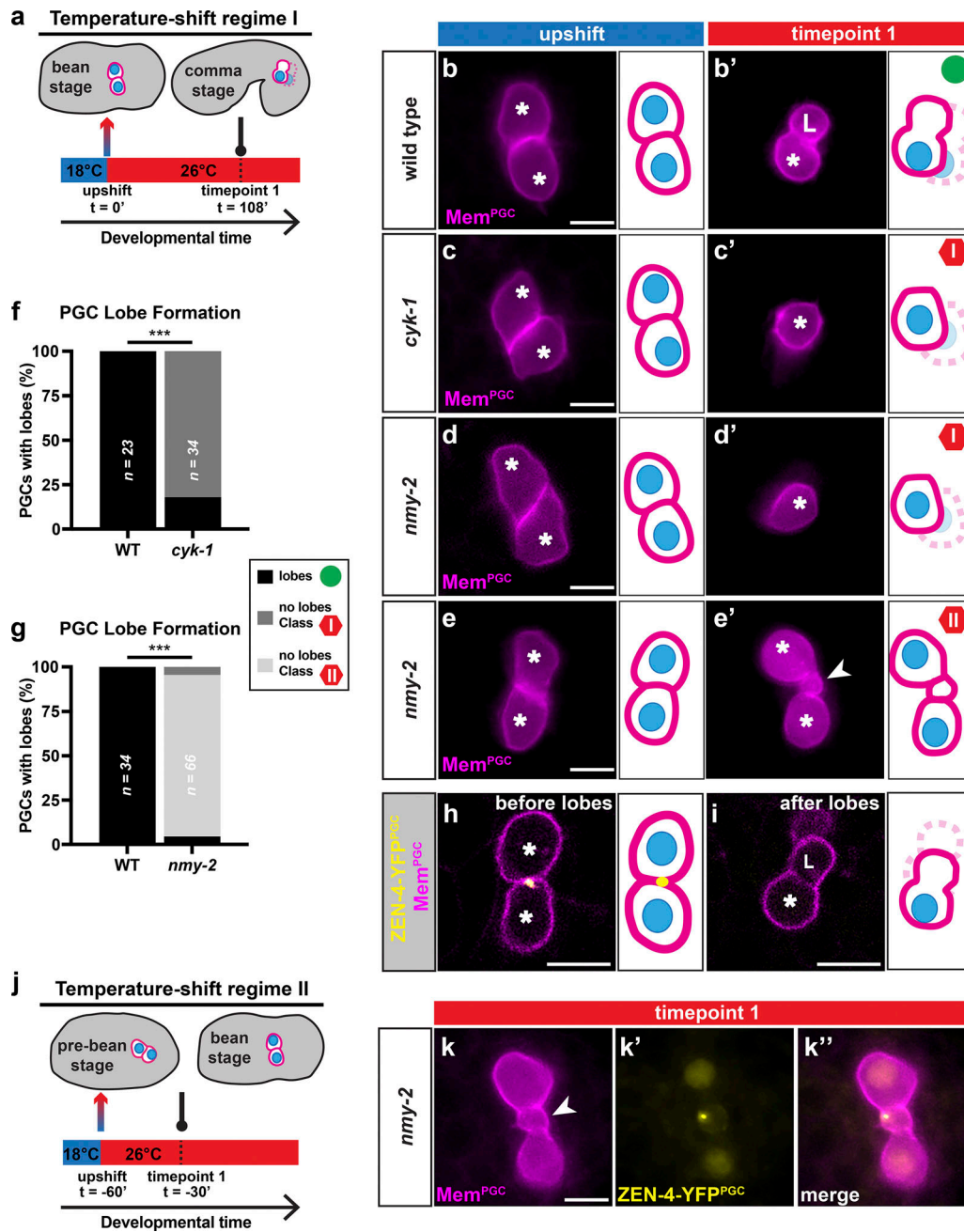
Figure 2. **cyk-1 and nmy-2 are required for PGC lobe formation. (a)** Temperature-shift regime I used for experiments shown in b-g. **(b–e')** Left: PGCs in embryos of the indicated genotype at the time of upshift. Right: PGCs in embryos of the indicated genotype at time point 1 (t = 108 min). Class I and Class II embryos are shown for *nmy-2*, with the expanded intercellular bridge indicated in e' (arrowhead). **(f and g)** Quantification of *cyk-1* (four combined experiments) and *nmy-2* (10 combined experiments) mutant PGC lobe formation compared with that of WT embryos on the same microscope slides. **(h and i)** ZEN-4-YFP^PGC in PGCs before and after lobe formation; yellow dot in schematic indicates a focus of ZEN-4-YFP^PGC. **(j)** Temperature-shift regime II, used for the experiment shown in k. **(k–k'')** *nmy-2* mutant embryo subjected to temperature-shift regime II showing an expanded intercellular bridge (arrowhead) marked with ZEN-4-YFP^PGC. ***, P < 0.0001, Fisher's exact test. * indicates nuclear position, and L indicates the lobe. Scale bar, 5 µm.

NOP-1, rather than centralspindlin, is required for PGC lobe formation

Two mechanisms have been shown to promote ECT-2 activation during cytokinesis. The predominant ECT-2 activator is centralspindlin (Basant and Glotzer, 2018), whereas the novel protein NOP-1 contributes to ECT-2 activation redundantly but, on its own, is dispensable for cytokinesis (Tse et al., 2012). *C. elegans*

centralspindlin is a complex of CYK-4/MgcRacGAP and ZEN-4/MKLP1 (Mishima et al., 2002). Temperature-sensitive alleles of *zen-4* and *cyk-4* that disrupt the interaction between the two proteins [*zen-4(or153ts)*] or that prevent CYK-4 membrane localization [*cyk-4(or749ts)*] effectively block cytokinesis (Davies et al., 2014; Pavicic-Kaltenbrunner et al., 2007; Zhang and Glotzer, 2015). Surprisingly, *cyk-4* or *zen-4* embryos that were
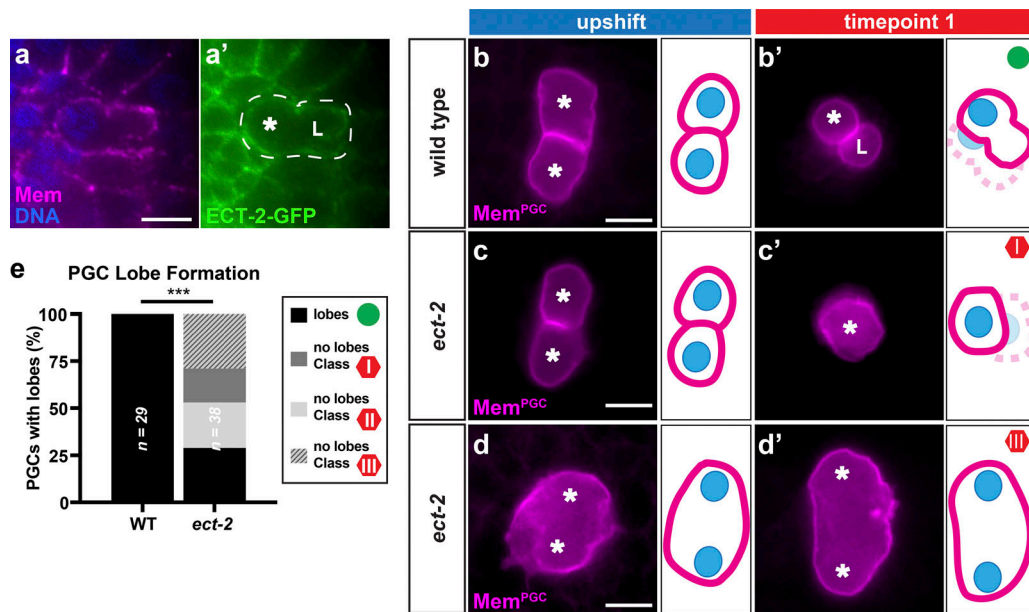
Maniscalco et al.
Primordial germ cell remodeling by a contractile ring

Journal of Cell Biology
https://doi.org/10.1083/jcb.201906185

4

Figure 3. ***ect-2* is required for PGC lobe formation. (a and a')** ECT-2-GFP enrichment at the cortex of a PGC (dashed line) in a comma-stage embryo. **(b–d')** PGCs in control and *ect-2* mutants subjected to temperature-shift regime I. Class I and Class III phenotypes are shown. **(e)** Quantification of *ect-2* mutant PGC lobe formation pooled from four experiments. ***, P < 0.0001, Fisher's exact test. * indicates nuclear position, and L indicates the lobe. Scale bar, 5 µm.

upshifted using temperature-shift regime I showed normal PGC lobe formation (Fig. 4, b', c', f, and g). To confirm that similar temperature upshifts of *cyk-4* and *zen-4* were able to block cytokinesis, we examined division of P_4, the parent cell of the PGCs. The majority of *cyk-4* or *zen-4* mutant embryos upshifted before P_4 mitosis failed in P_4 cytokinesis (Fig. S2, a–f). These results, together with the lack of ZEN-4 localization at PGC lobe necks (Fig. 2 i), strongly suggest that PGC lobe formation does not require centralspindlin.

To determine whether ECT-2 might be activated instead by NOP-1, we examined *nop-1* mutant embryos, which are mostly viable (Rose et al., 1995). In *nop-1* mutant embryos, most PGCs lacked lobes; however, a few developed defects in the maintenance of the PGC intercellular bridge that we noted in *nmy-2* and *ect-2* mutant embryos (Fig. 4, e' and h). Thus, ECT-2 regulation differs during PGC lobe formation and cytokinesis: PGC lobe formation requires NOP-1, whereas cytokinesis requires centralspindlin.

Polarized PGC nuclear movements predict the site of lobe formation

Since the PGC nucleus is always opposite the lobe, we wondered whether it moves to a stereotypical location within the cell before lobe formation. We examined nuclear dynamics by filming embryos expressing Mem^{PGC} and a PGC-specific nuclear marker (GFP-H2B). To quantify nuclear position relative to the PGC cell body, we defined the PGC-PGC contact as the medial side of each PGC and the opposite end of each cell as the lateral side. Prior to lobe formation, the nucleus was positioned near the center of the PGC (Fig. 5, a and b). As PGCs lengthened before lobe formation (Fig. 1 a'), the nucleus migrated to the lateral edge (Fig. 5, c and d). Centrosomes, which we detected using SPD-2-GFP, were

invariably localized on the lateral-facing side of the nucleus (27/27 PGCs; Fig. 5, g–i). However, time-lapse movies of the plus-end binding protein EBP-2-GFP (Sallee et al., 2018) revealed that centrosomes in PGCs do not function as major microtubule organizing centers; rather, microtubules appeared to grow predominantly from the plasma membrane (38/38 embryos; Video 3). These observations raise the possibility that nuclear asymmetry and lobe formation are coupled and that nuclear movement may drive PGC elongation.

After nuclear migration, PGC lobes invariably formed toward the medial side of the cell rather than extending laterally (Fig. 5, e and f), suggesting that the nucleus might locally inhibit lobe formation. To determine if and where lobes form when the nucleus is abnormally positioned, we used *zen-4* mutants to create embryos containing a binucleate PGC. For these experiments, we upshifted *zen-4* mutants before the P_4 cell division (t = 0 min) and captured images at two subsequent time points (Fig. 5 j). At time point 1 (t = 110 min), the P_4 cell had completed division in all WT embryos (17/17) but had not yet formed lobes (Fig. 5, l–l'). At time point 2 (t = 300 min), PGCs in WT embryos had formed lobes (17/17; Fig. 5, m–m'). Nearly all (39/40) *zen-4* embryos exposed to this temperature-shift regime contained a single binucleate PGC at time point 1 (Fig. 5, n–n'), and by time point 2, the binucleate PGC developed deep lobe-like invaginations on the side of the cell opposite the clustered nuclei (33/39 embryos; Fig. 5, k and o–o'). Movies captured with higher time resolution revealed that the paired nuclei moved to one side of the PGC before lobe formation was initiated on the opposite side (7/7 embryos; Fig. S3 a). As in WT PGCs, NMY-2-YFP^{PGC} accumulated at the base of lobe necks in binucleate *zen-4* PGCs (Fig. S3 b'', arrowheads). These findings are consistent with a role for nuclei in positioning the PGC lobe.
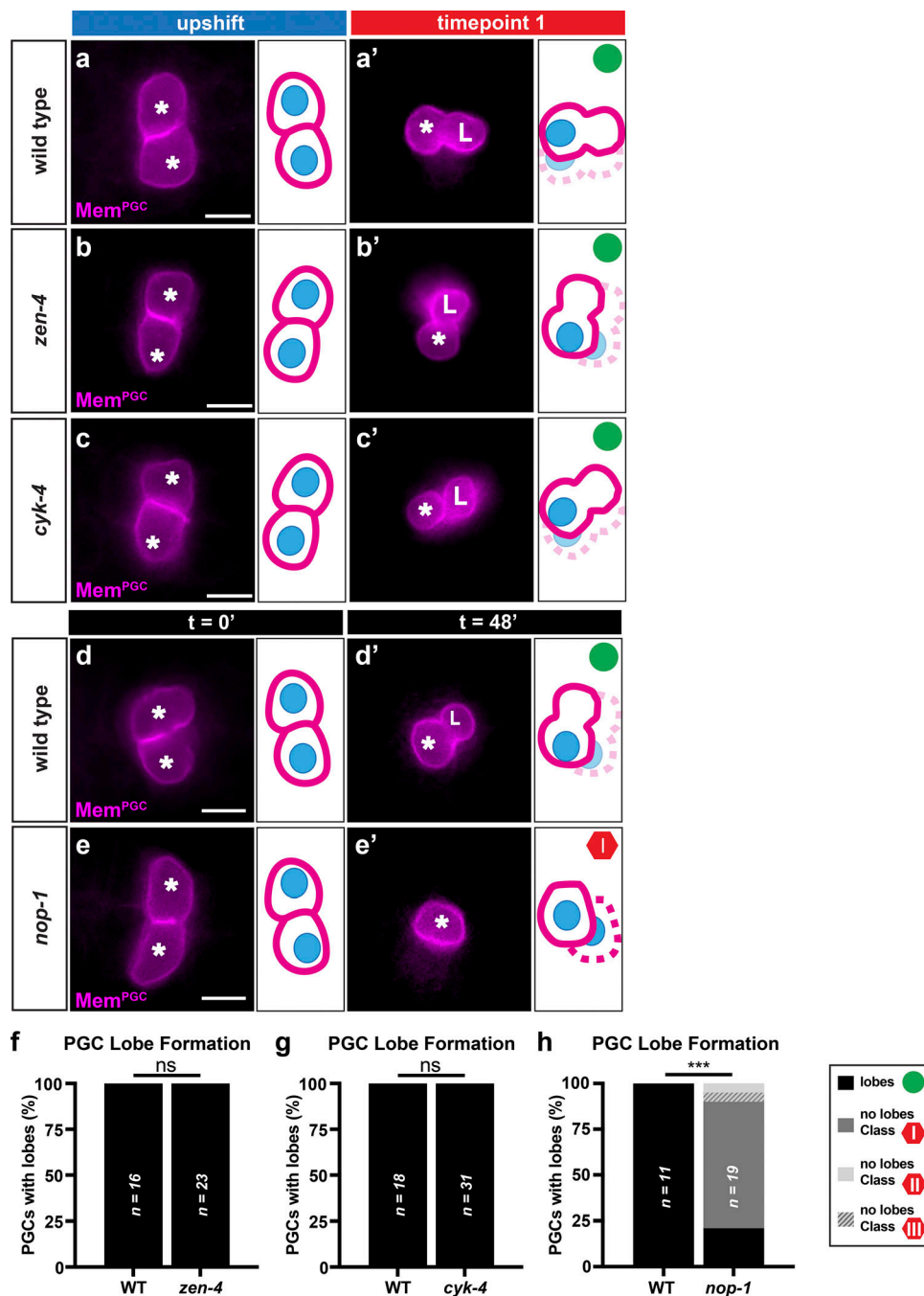
Figure 4. **nop-1, but not centralspindlin, is required for PGC lobe formation. (a–c')** Control, *zen-4*, and *cyk-4* mutant PGCs subjected to temperature-shift regime I. **(d–e')** PGCs in control and *nop-1* mutants at the indicated time points; t = 0 is just before lobes form in the control. **(f–h)** Quantification of *zen-4* (combined from three experiments), *cyk-4* (combined from four experiments), and *nop-1* (combined from two experiments) phenotypes. ns, not significant. * indicates nuclear position, and L indicates the lobe. ***, P < 0.0001, Fisher's exact test. Scale bar, 5 µm.

A model for cellular compartment formation

We suggest the following model for PGC lobe formation. First, the PGC nucleus migrates to the lateral edge of the PGC, which we propose induces the formation of a contractile ring between the nucleus and the medial side of the cell. Ring constriction causes the plasma membrane to ingress, creating the lobe. Our findings reveal clear similarities and differences in the regulation of PGC lobe and cytokinetic contractile rings. One similarity is the requirement for RhoA activity (Jantsch-Plunger et al., 2000). However, a key difference is that PGC lobe formation occurs independently of centralspindlin, which is essential for cytokinesis. Whereas centralspindlin functions in cytokinesis by activating ECT-2, this role appears to be largely fulfilled in PGCs by NOP-1. The dispensability of centralspindlin may not seem surprising given that PGCs are nonmitotic and therefore lack a spindle. However, a spindle-independent role for central-spindlin component CYK-4 was recently described in oocyte cellularization (Lee et al., 2018).
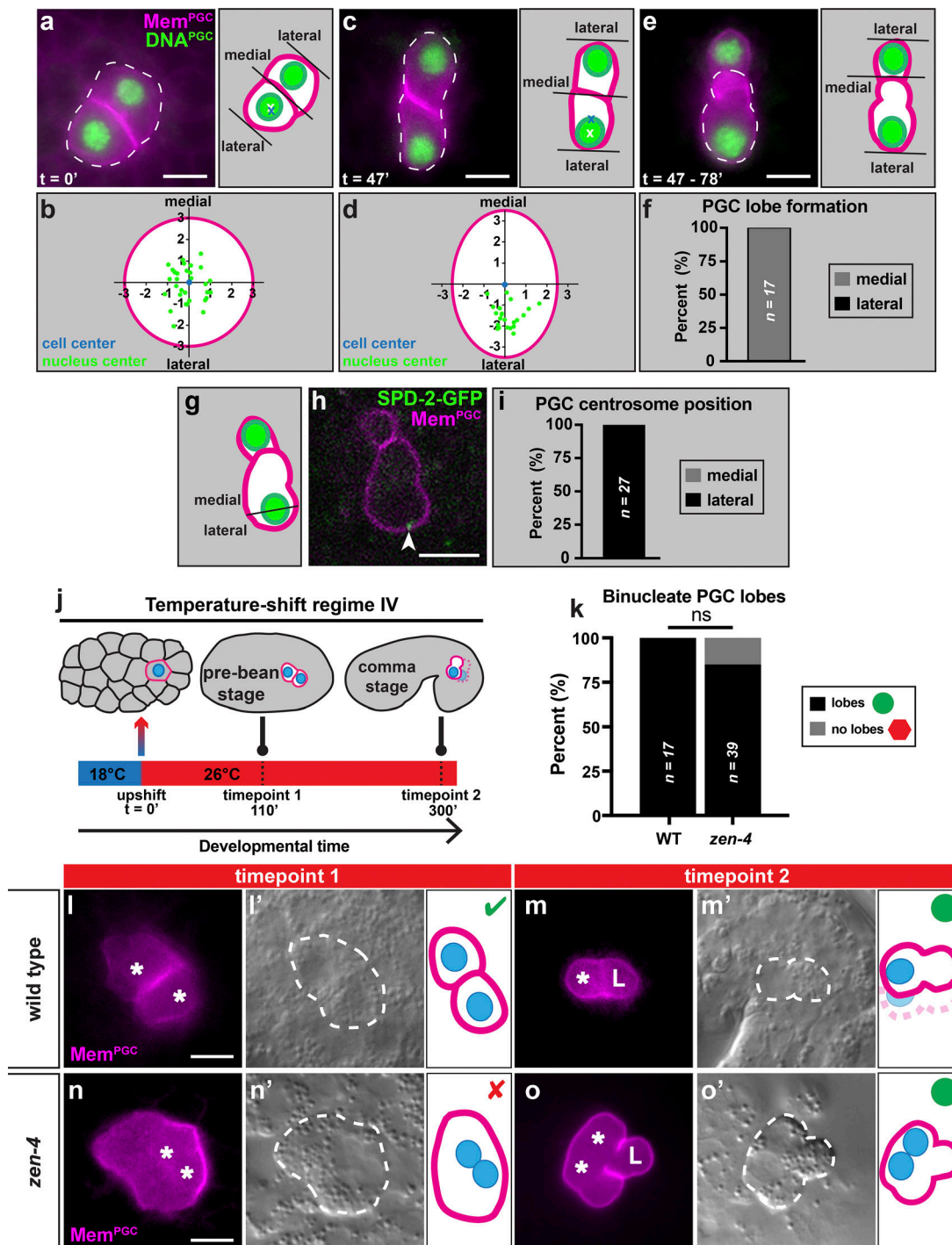
Maniscalco et al.
Primordial germ cell remodeling by a contractile ring

Journal of Cell Biology 6
https://doi.org/10.1083/jcb.201906185

Figure 5. **PGC nuclear position predicts the site of lobe formation. (a, c, and e)** PGC nuclei before (a), just before (c), and just after (e) lobe formation; dashed lines indicate PGCs. **(b and d)** Quantification of PGC nuclear positions before the period of lobe formation (b) and just before lobe formation (d). The center of the nucleus is shown relative to the center of the PGC, with scaling indicating distance in microns. Approximate position of the PGC plasma membrane is shown. **(f)** Position of lobe formation relative to the medial-lateral axis. **(g–i)** Centrosome position (arrowhead in h) in PGCs determined using the SPD-2-GFP marker. **(j)** Temperature-shift regime IV, used for experiment in l–o'. **(k)** Quantification of lobe formation in binucleate *zen-4* mutant embryos pooled from six experiments. **(l–o')** Mononucleate control and binucleate *zen-4* PGCs. DIC images reveal nuclear localization (dashed lines outline PGCs, nuclei are in clear regions). Green checkmark represents successful P_4 division, red X indicates failed P_4 division. * indicates nuclear position, and L indicates the lobe. ns, not significant. Fisher's exact test. Scale bar, 5 µm.

What provides the spatial information that positions the lobe contractile ring? PGC-PGC and PGC–somatic cell interactions are not required for lobe formation, as lobe formation occurs in a single binucleate PGC (Fig. 5, n–o') or in PGCs cultured in isolation (Abdu et al., 2016). Because the lobe contractile ring always forms on the medial side of the asymmetrically positioned nucleus, we consider it likely that the nucleus or attached centrosomes contribute to contractile ring positioning. If so, PGC

Maniscalco et al.
Primordial germ cell remodeling by a contractile ring

Journal of Cell Biology
https://doi.org/10.1083/jcb.201906185

7

lobe formation may be mechanistically similar to pseudocleavage formation, which occurs in the *C. elegans* zygote in the absence of a mitotic spindle and also depends on NOP-1 (Albertson, 1984; Rose et al., 1995; Tse et al., 2012). Pseudocleavage is prompted by a cue from the centrosome, which inhibits actomyosin contractility at the posterior cortex, causing actomyosin to contract anteriorly into a cap that constricts into a furrow at its posterior border (Cowan and Hyman, 2004; Hird, 1996; Munro et al., 2004; Strome, 1986). It is plausible that centrosomes also induce formation of the PGC contractile ring since they invariably face away from the site of lobe formation, although our EBP-2-GFP imaging experiments suggest that they are unlikely to do so by functioning as major sites of microtubule polymerization.

PGC lobe formation also shares similarities and differences with erythroblast enucleation. In erythroblasts, the nucleus migrates to one side of the cell, which subsequently forms and constricts an equatorial contractile ring to separate the cytoplasmic compartment from the nuclear compartment (Moras et al., 2017; Ovchynnikova et al., 2018). However, a key difference is in how the contractile ring is regulated. Whereas erythroblasts require Rac to form the enucleation contractile ring (Ji et al., 2008; Konstantinidis et al., 2012), our findings implicate RhoA. Thus, while contractile rings similar to those that separate cells during cytokinesis can be reemployed during interphase to create cellular compartments used for remodeling, divergent regulatory inputs can direct their formation.

Cannibalism of the PGC lobes dramatically reduces PGC volume and mitochondrial content (Abdu et al., 2016). While the importance of PGC remodeling is unknown, one role may be to eliminate most PGC mitochondria, which are high in potentially damaging superoxides relative to mitochondria in other embryonic cells (Abdu et al., 2016). It is interesting to note that *nop-1* mutants have reduced fecundity and ~20% embryonic lethality (Rose et al., 1995; Tse et al., 2012), raising the possibility that these phenotypes could be consequences of defects in PGC remodeling.

Materials and methods
Strains
C. elegans strains were maintained at room temperature on nematode growth medium plates seeded with *Escherichia coli* strain OP50. Temperature-sensitive strains and FT1909 were maintained at 15°C. The following strains were used: DP38: *unc-119(ed3)* (Maduro and Pilgrim, 1995), FT404: *ect-2(gk44); unc-119(ed3); xnIs162* [*Pect-2::ect-2-gfp, unc-119(+)*], FT1258: *him-8(e1489); xnIs360* [*Pmex-5::mCherry-PH::nos-2³'ᵁᵀᴿ, unc-119(+)*] *zuIs70* [*Pend-1::gfp-caax, unc-119(+)*], FT1614: *xnIs360; Ppie-1::gfp-H2B::nos-2³'ᵁᵀᴿ, unc-119(+)* (D'Agostino et al., 2006), FT1729: *avr-14(ad1302); xnSi49* [*Pmex-5::nmy-2-yfp::nos-2³'ᵁᵀᴿ, unc-119(+)*]; *unc-119(ed3); avr-15(ad1051) glc-1(pk54)*, FT1749: *xnSi49; xnIs360*, FT1851: *zen-4(or153ts); xnIs360*, FT1852: *nmy-2(ne3409ts); xnIs360; him-8(e1489)*, FT1853: *cyk-1(or596ts); xnIs360*, FT1909: *xnIs360; zuIs178* [*Phis-72::his-72-gfp::his-72³'ᵁᵀᴿ, unc-119(+)*], FT1927: *cyk-4(or749ts); xnIs360*, FT1938: *itSi922* [*Pspd-2::gfp-spd-2, unc-119(+)*]; *xnIs360*, FT1974: *nop-1(it142); xnIs360; zuIs70,*

FT2000: *xnSi50* [*Pmex-5::zen-4-yfp::nos-2³'ᵁᵀᴿ, unc-119(+)*]; *xnIs360*, FT2051: *nmy-2(ne3409ts); xnSi50; xnIs360*, FT2088: *ebp-2(wow47: ebp-2-gfp); xnIs360*, FT2096: *nmy-2(cp13[nmy-2-gfp + LoxP]); xnSi49; xnIs360*, FT2107: *zen-4(or153ts); xnSi49; xnIs360*, FT2108: *ect-2(ax751ts); xnIs360*, FT2109: *unc-119(ed3); xnIs101* [*Ppie-1::gfp-Moesin::nos-2³'ᵁᵀᴿ, unc-119(+)*]; *xnIs360*, and WM186: *avr-14(ad1302); ttTi5605; unc-119(ed3); avr-15(ad1051) glc-1(pk54); neEx15* [*myo-2::RFP, myo-2::avr-15(+), unc-119(+)*] (Shirayama et al., 2012).

Gene, transgene, and fusion protein nomenclature in the text and figures relates to the following alleles and transgenes: *cyk-1* = *cyk-1(or596ts), cyk-4* = *cyk-4(or749ts), ect-2* = *ect-2(ax751ts), nmy-2* = *nmy-2(ne3409ts), nop-1* = *nop-1(it142), zen-4* = *zen-4(or153ts),* F-actin^PGC = *xnIs101* [*Ppie-1::gfp-Moesin::nos-2³'ᵁᵀᴿ, unc-119(+)*], Mem^PGC = *xnIs360* [*Pmex-5::mCherry-PH::nos-2³'ᵁᵀᴿ, unc-119(+)*], NMY-2-GFP = *nmy-2(cp13[nmy-2::GFP + LoxP])*, NMY-2-YFP^PGC = *xnSi49* [*Pmex-5::nmy-2-yfp::nos-2³'ᵁᵀᴿ, unc-119(+)*], and ZEN-4-YFP^PGC = *xnSi50* [*Pmex-5::zen-4-yfp::nos-2³'ᵁᵀᴿ, unc-119(+)*].

Transgene construction
Pmex-5::nmy-2-yfp::nos-2³'ᵁᵀᴿ was assembled from plasmid *Pmex-5::hmr-1-gfp::nos-2³'ᵁᵀᴿ*, which was constructed using Multisite Gateway (Invitrogen) from vector pCFJ150 (Addgene #19329) (Frøkjær-Jensen et al., 2008), 5′ entry clone pJA252 (*Pmex-5*; Addgene #21512; Zeiser et al., 2011), middle entry clone pJN527 (*hmr-1-gfp*; Chihara and Nance, 2012), and 3′ entry clone pDC10 (*nos-2* 3′ UTR; Chihara and Nance, 2012). *hmr-1-gfp* was replaced with *nmy-2* genomic sequence and *yfp* in a three-fragment Gibson Assembly reaction (Gibson et al., 2009).

Pmex-5::zen-4-yfp::nos-2³'ᵁᵀᴿ was constructed from *Pmex-5::nmy-2-yfp::nos-2³'ᵁᵀᴿ*, replacing *nmy-2* with *zen-4* genomic sequence via Gibson Assembly.

Ppie-1::gfp-Moesin::nos-2³'ᵁᵀᴿ was constructed from vector pKS111-His (*Ppie-1::gfp-Histone::nos-2³'ᵁᵀᴿ*; a gift from Kuppuswamy Subramaniam; D'Agostino et al., 2006). pKS111-His was digested with *Spe*I to remove the Histone H2B coding region. cDNA encoding amino acids 438–575 of *Drosophila melanogaster* Moesin (isoform D) was amplified by PCR using primers containing *Spe*I restrictions sites and ligated with the pKS111-His vector fragment.

Worm transformation
Ppie-1::gfp-Moesin::nos-2³'ᵁᵀᴿ was integrated through microparticle bombardment using a Bio-Rad Biolistic PDS-1000/HE gene gun outfitted with a Hepta adaptor (Praitis et al., 2001). DNA (1–2 µg) was precipitated onto 1.0-µm-diameter gold beads (1652263; Bio-Rad) and bombarded directly onto an unseeded 10-cm agar plate containing a uniform lawn of young adult *unc-119(ed3)* worms. Bombarded worms were transferred to ten 10-cm peptone-enriched agar plates seeded with *E. coli* strain NA22 and allowed to starve. Twelve non-Unc worms were singled from each plate containing transformants and were allowed to self-fertilize to identify homozygous integrants, which were scored for GFP expression.

Pmex-5::nmy-2-yfp::nos-2³'ᵁᵀᴿ and *Pmex-5::zen-4-yfp::nos-2³'ᵁᵀᴿ* were microinjected as described (Mello et al., 1991) into WM186 worms lacking the *neEx15* extrachromosomal array at a

Maniscalco et al.
Primordial germ cell remodeling by a contractile ring

Journal of Cell Biology   8
https://doi.org/10.1083/jcb.201906185

concentration of 20 ng/µl together with 50 ng/ml each of pRF4 [*rol-6(su1006)*] (Mello et al., 1991), pCCM416 [*Pmyo-2::avr-15*] (a gift from Craig Mello; Shirayama et al., 2012), and pJL44 [*Phsp16.48::MosTase::glh-2³'ᵁᵀᴿ*] (19333; Addgene; Frokjær-Jensen et al., 2008). A transmitting extrachromosomal line was isolated by its Rol phenotype and integrated using the heat-shock method (Frøkjær-Jensen et al., 2008; Shirayama et al., 2012). Briefly, several thousand transgenic worms were heat shocked at 35°C for 1.5 h and grown for two generations, and F3 embryos were plated onto NGM agar plates containing 2 ng/µl of ivermectin. After 3 d, surviving non-Unc non-Rol worms were picked from each plate and tested for homozygosity of the insertion and for YFP expression.

Immunostaining

Embryos were dissected on poly-L-lysine–coated slides, freeze cracked, and fixed in −20°C MeOH (20 min) and 3.7% formaldehyde in salts (50 mM Pipes, 25 mM Hepes, 10 mM EGTA, and 2 mM $MgCl_2$; 5 min) before washing in PBS-Tween and immunostaining directly on slides in PBS-Tween containing 1% IgG-free BSA (001–000-162; Jackson ImmunoResearch). The following primary antibodies were used: chicken anti-GFP 1:10 (GFP-1010; Aves Labs), rabbit anti-UNC-59 1:100 (Maddox et al., 2005; a gift from Karen Oegema), rabbit anti-ANI-1 1:100 (Maddox et al., 2005; a gift from Karen Oegema), and mouse anti-FRM-1 1:1,000 (Choi et al., 2011; a gift from Nam Jeong Cho). The following secondary antibodies were used: AlexaFluor 488 goat anti-chicken IgY (H+L) (A-11039; Thermo Fisher Scientific), Cy3 donkey anti-rabbit IgG (H+L) (711–165-152, lot 86701; Jackson ImmunoResearch), and Cy5 donkey anti-mouse IgG (H+L) (715–175-151, lot 76920; Jackson ImmunoResearch). After washing and incubating with 4′,6-diamidino-2-phenylindole, embryos were mounted in 90% glycerol containing 1,4-diazabicyclo [2.2.2]octane (D27802; Sigma-Aldrich) anti-fade agent.

Microscopy and image analysis

Live embryos mounted on 4% agarose pads in M9 medium and fixed embryos attached directly to slides and mounted in 90% glycerol with 1,4-diazabicyclo[2.2.2]octane anti-fade agent were imaged either on a Zeiss AxioImager.A2 using a 40× Plan-Neofluar 1.3 NA or 63× Plan-Apochromat 1.4 NA oil-immersion objective, Axiocam 503 mono camera, Uniblitz shutter (Vincent Associates), and Zen software (Zeiss) or on a Leica TCS SP8 confocal microscope equipped with HyD detectors using a 63× 1.4 NA oil-immersion objective lens and LAS AF software. Imaging was performed at room temperature except for temperature-sensitive mutants, where temperatures at each time point are indicated. Images of fixed embryos were deconvolved using ZEN software and the Fast Iterative method. Brightness, contrast, and gamma level adjustments, as well as image resizing and cropping, were performed using Fiji (National Institutes of Health) and Photoshop (Adobe).

Time-lapse imaging of centrosomes and microtubule growth

A Nikon Ti2-E microscope with CSU-W1 Spinning Disk, 100X CFI SR HP PlanApochromat 1.35 NA silicone immersion objective, and IXON Life 888 Dual EMCCD camera and NIS Elements software were used for imaging centrosomes and microtubule growth in PGCs. For centrosomes, 12-µm image stacks (1-µm step size) of Memᴾᴳᶜ and SPD-2-GFP were captured every 5 min for ~1 h, through the period of lobe formation. For determining the site and direction of microtubule growth, Memᴾᴳᶜ and EBP-2-GFP were imaged continuously for 20 s in a single plane through the center of the PGCs. Microtubule growth was determined by following EBP-2-GFP puncta using the MTrackJ Fiji macro with manual annotation of tracks (Meijering et al., 2012).

Temperature-shift and *nop-1* imaging experiments

Worms were dissected at the permissive temperature (18°C), and two-cell embryos collected over a ~10-min period were mounted on 4% agar pads in M9. Control and experimental embryos were mounted in separate, nearby clusters on the same slide for every experiment. Slides were transferred to a ~24°C metal plate in the microscope room at the indicated time and immediately mounted for microscopy on a Zeiss AxioImager.Z2 compound microscope. Temperature of the samples was maintained at the restrictive temperature (26°C ± 0.5°C) using room temperature control and an HLS-1p objective heater and thermistor probe (Cell MicroControls), which was monitored throughout the duration of the experiment. mCherry and differential interference contrast (DIC) image stacks were acquired immediately and again at the indicated time. The presence of a nucleus was scored using DIC images.

To test temperature-sensitive mutants for a role in PGC lobe formation (temperature-shift regime I), embryos were shifted from the permissive temperature to the restrictive temperature 6 h and 30 min after the two-cell stage, and the final image was taken at 8 h 28 min. Samples were discarded if control embryos mounted on the same slide failed in lobe formation.

To examine whether *nmy-2* Class II mutants (temperature-shift regime II) had a defect in maintaining the connection between PGCs, embryos were shifted from the permissive temperature to the restrictive temperature 5 h and 30 min after the two-cell stage. The final image was taken at 6 h, a stage before PGCs form lobes in WT control embryos.

To test *zen-4* and *cyk-4* mutants for a role in P_4 division (temperature-shift regime III), embryos were shifted from the permissive temperature to the restrictive temperature 2 h after the two-cell collections, and the final image was captured at 3 h 50 min. Samples were discarded if control embryos mounted on the same slide failed in P_4 division.

To examine lobe formation in binucleate embryos (temperature-shift regime IV), *zen-4* embryos were shifted from the permissive temperature to the restrictive temperature 2 h after the two-cell collections, time point 1 was captured at 3 h 50 min, and time point 2 was captured at 7 h. For experiments with higher time resolution, DIC and mCherry image stacks were captured every 5 min, beginning at time point 1 above. 2 × 2 pixel binning was used to reduce fluorescence exposure times.

To examine lobe formation in *nop-1* mutant embryos, control (FT1258) and *nop-1(it142)* mutant (FT1974) two-cell embryos were dissected and kept at 25°C. The first time point was captured at 4 h 45 min after the two-cell stage and every subsequent 8 min until 5 h 33 min (t = 48 min after the first time point).

Nuclear movement experiments

Worms were grown at 25°C, and two-cell embryos that were collected over a ~10-min period were mounted on 4% agar pads. mCherry and GFP image stacks were acquired on a Zeiss Axio-Imager microscope 4 h and 7 min (t = 0 min) after initial dissection and again at the indicated times. To determine nuclear localization within the PGC, the center of the cell and the center of the nucleus were measured at the first two time points using a custom macro in ImageJ. Positions were plotted on a graph with the origin representing the center of the PGC.

Statistical analysis

Sample sizes and number of experiments pooled for data shown in the graphs are indicated directly in the figures and figure legends. Fisher's exact test was used to compare mutant embryos with control embryos. Controls mounted on the same slide were performed for each mutant genotype. P values >0.05 were considered not significant; the P value of significant differences is indicated in the figure legends.

Online supplemental material

Fig. S1 (related to Fig. 1) shows NMY-2-YFP^{PGC} accumulating at lobe necks as they first begin to ingress. Fig. S2 (related to Fig. 4) shows that the *cyk-4* and *zen-4* temperature-sensitive mutants block division of the P$_4$ cell at the temperature used to test whether they are required for PGC lobe formation. Fig. S3 (related to Fig. 5) shows that asymmetric nuclear positioning occurs before lobe formation in *zen-4* binucleate PGCs and that NMY-2-YFP^{PGC} localizes to the neck of lobes in *zen-4* binucleate PGCs. Video 1 (related to Fig. 1) shows Mem^{PGC} during PGC lobe formation in a WT embryo. Video 2 (related to Fig. 1) shows a rotated image stack of NMY-2-YFP^{PGC} at a PGC lobe neck to illustrate that it forms a ring. Video 3 (related to Fig. 5) shows dynamics and tracks of the microtubule plus-end binding protein EBP-2-GFP to demonstrate where microtubule growth occurs in PGCs.

Author contributions: C. Maniscalco and J. Nance conceptualized the project. C. Maniscalco, A.E. Hall, and J. Nance performed experiments and analyzed and interpreted the data. C. Maniscalco and J. Nance wrote the original draft, and A.E. Hall and J. Nance wrote the revised manuscript.

References

Abdu, Y., C. Maniscalco, J.M. Heddleston, T.L. Chew, and J. Nance. 2016. Developmentally programmed germ cell remodelling by endodermal cell cannibalism. *Nat. Cell Biol.* 18:1302–1310. https://doi.org/10.1038/ncb3439

Albertson, D.G. 1984. Formation of the first cleavage spindle in nematode embryos. *Dev. Biol.* 101:61–72. https://doi.org/10.1016/0012-1606(84)90117-9

Basant, A., and M. Glotzer. 2018. Spatiotemporal Regulation of RhoA during Cytokinesis. *Curr. Biol.* 28:R570–R580. https://doi.org/10.1016/j.cub.2018.03.045

Bohnert, K.A., A.H. Willet, D.R. Kovar, and K.L. Gould. 2013. Formin-based control of the actin cytoskeleton during cytokinesis. *Biochem. Soc. Trans.* 41:1750–1754. https://doi.org/10.1042/BST20130208

Breucker, H., E. Schäfer, and A.F. Holstein. 1985. Morphogenesis and fate of the residual body in human spermiogenesis. *Cell Tissue Res.* 240:303–309. https://doi.org/10.1007/BF00222339

Chihara, D., and J. Nance. 2012. An E-cadherin-mediated hitchhiking mechanism for *C. elegans* germ cell internalization during gastrulation. *Development.* 139:2547–2556. https://doi.org/10.1242/dev.079863

Choi, B., J. Kang, Y.S. Park, J. Lee, and N.J. Cho. 2011. A possible role for FRM-1, a *C. elegans* FERM family protein, in embryonic development. *Mol. Cells.* 31:455–459. https://doi.org/10.1007/s10059-011-0323-0

Cinalli, R.M., and R. Lehmann. 2013. A spindle-independent cleavage pathway controls germ cell formation in Drosophila. *Nat. Cell Biol.* 15:839–845. https://doi.org/10.1038/ncb2761

Cowan, C.R., and A.A. Hyman. 2004. Centrosomes direct cell polarity independently of microtubule assembly in *C. elegans* embryos. *Nature.* 431:92–96. https://doi.org/10.1038/nature02825

D'Agostino, I., C. Merritt, P.L. Chen, G. Seydoux, and K. Subramaniam. 2006. Translational repression restricts expression of the *C. elegans* Nanos homolog NOS-2 to the embryonic germline. *Dev. Biol.* 292:244–252. https://doi.org/10.1016/j.ydbio.2005.11.046

Davies, T., S.N. Jordan, V. Chand, J.A. Sees, K. Laband, A.X. Carvalho, M. Shirasu-Hiza, D.R. Kovar, J. Dumont, and J.C. Canman. 2014. High-resolution temporal analysis reveals a functional timeline for the molecular regulation of cytokinesis. *Dev. Cell.* 30:209–223. https://doi.org/10.1016/j.devcel.2014.05.009

Dickinson, D.J., J.D. Ward, D.J. Reiner, and B. Goldstein. 2013. Engineering the *Caenorhabditis elegans* genome using Cas9-triggered homologous recombination. *Nat. Methods.* 10:1028–1034. https://doi.org/10.1038/nmeth.2641

Frøkjær-Jensen, C., M.W. Davis, C.E. Hopkins, B.J. Newman, J.M. Thummel, S.P. Olesen, M. Grunnet, and E.M. Jorgensen. 2008. Single-copy insertion of transgenes in *Caenorhabditis elegans*. *Nat. Genet.* 40:1375–1383. https://doi.org/10.1038/ng.248

Fukuyama, M., A.E. Rougvie, and J.H. Rothman. 2006. *C. elegans* DAF-18/PTEN mediates nutrient-dependent arrest of cell cycle and growth in the germline. *Curr. Biol.* 16:773–779. https://doi.org/10.1016/j.cub.2006.02.073

Gibson, D.G., L. Young, R.Y. Chuang, J.C. Venter, C.A. Hutchison III, and H.O. Smith. 2009. Enzymatic assembly of DNA molecules up to several hundred kilobases. *Nat. Methods.* 6:343–345. https://doi.org/10.1038/nmeth.1318

Glotzer, M. 2017. Cytokinesis in Metazoa and Fungi. *Cold Spring Harb. Perspect. Biol.* 9:a022343. https://doi.org/10.1101/cshperspect.a022343

Goupil, E., R. Amini, D.H. Hall, and J.C. Labbé. 2017. Actomyosin contractility regulators stabilize the cytoplasmic bridge between the two primordial germ cells during *Caenorhabditis elegans* embryogenesis. *Mol. Biol. Cell.* 28:3789–3800. https://doi.org/10.1091/mbc.e17-08-0502

Green, R.A., E. Paluch, and K. Oegema. 2012. Cytokinesis in animal cells. *Annu. Rev. Cell Dev. Biol.* 28:29–58. https://doi.org/10.1146/annurev-cellbio-101011-155718

Hird, S. 1996. Cortical actin movements during the first cell cycle of the *Caenorhabditis elegans* embryo. *J. Cell Sci.* 109:525–533.

Jantsch-Plunger, V., P. Gönczy, A. Romano, H. Schnabel, D. Hamill, R. Schnabel, A.A. Hyman, and M. Glotzer. 2000. CYK-4: A Rho family gtpase activating protein (GAP) required for central spindle formation and cytokinesis. *J. Cell Biol.* 149:1391–1404. https://doi.org/10.1083/jcb.149.7.1391

Ji, P., S.R. Jayapal, and H.F. Lodish. 2008. Enucleation of cultured mouse fetal erythroblasts requires Rac GTPases and mDia2. *Nat. Cell Biol.* 10:314–321. https://doi.org/10.1038/ncb1693

Konstantinidis, D.G., S. Pushkaran, J.F. Johnson, J.A. Cancelas, S. Manganaris, C.E. Harris, D.A. Williams, Y. Zheng, and T.A. Kalfa. 2012. Signaling and cytoskeletal requirements in erythroblast enucleation. *Blood.* 119:6118–6127. https://doi.org/10.1182/blood-2011-09-379263

Kosako, H., T. Yoshida, F. Matsumura, T. Ishizaki, S. Narumiya, and M. Inagaki. 2000. Rho-kinase/ROCK is involved in cytokinesis through the phosphorylation of myosin light chain and not ezrin/radixin/moesin proteins at the cleavage furrow. *Oncogene.* 19:6059–6064. https://doi.org/10.1038/sj.onc.1203987

Koury, S.T., M.J. Koury, and M.C. Bondurant. 1989. Cytoskeletal distribution and function during the maturation and enucleation of mammalian erythroblasts. *J. Cell Biol.* 109:3005–3013. https://doi.org/10.1083/jcb.109.6.3005

Lee, K.Y., R.A. Green, E. Gutierrez, J.S. Gomez-Cavazos, I. Kolotuev, S. Wang, A. Desai, A. Groisman, and K. Oegema. 2018. CYK-4 functions independently of its centralspindlin partner ZEN-4 to cellularize oocytes in germline syncytia. *eLife.* 7:e36919. https://doi.org/10.7554/eLife.36919

Liu, J., L.L. Maduzia, M. Shirayama, and C.C. Mello. 2010. NMY-2 maintains cellular asymmetry and cell boundaries, and promotes a SRC-dependent asymmetric cell division. *Dev. Biol.* 339:366–373. https://doi.org/10.1016/j.ydbio.2009.12.041

Maddox, A.S., B. Habermann, A. Desai, and K. Oegema. 2005. Distinct roles for two *C. elegans* anillins in the gonad and early embryo. *Development.* 132:2837–2848. https://doi.org/10.1242/dev.01828

Maduro, M., and D. Pilgrim. 1995. Identification and cloning of *unc-119*, a gene expressed in the *Caenorhabditis elegans* nervous system. *Genetics.* 141:977–988.

Martin, A.C., and B. Goldstein. 2014. Apical constriction: themes and variations on a cellular mechanism driving morphogenesis. *Development.* 141:1987–1998. https://doi.org/10.1242/dev.102228

Meijering, E., O. Dzyubachyk, and I. Smal. 2012. Methods for cell and particle tracking. *Methods Enzymol.* 504:183–200. https://doi.org/10.1016/B978-0-12-391857-4.00009-4

Mello, C.C., J.M. Kramer, D. Stinchcomb, and V. Ambros. 1991. Efficient gene transfer in *C.elegans*: extrachromosomal maintenance and integration of transforming sequences. *EMBO J.* 10:3959–3970. https://doi.org/10.1002/j.1460-2075.1991.tb04966.x

Mi-Mi, L., S. Votra, K. Kemphues, A. Bretscher, and D. Pruyne. 2012. Z-line formins promote contractile lattice growth and maintenance in striated muscles of *C. elegans*. *J. Cell Biol.* 198:87–102. https://doi.org/10.1083/jcb.201202053

Mishima, M., S. Kaitna, and M. Glotzer. 2002. Central spindle assembly and cytokinesis require a kinesin-like protein/RhoGAP complex with microtubule bundling activity. *Dev. Cell.* 2:41–54. https://doi.org/10.1016/S1534-5807(01)00110-1

Moras, M., S.D. Lefevre, and M.A. Ostuni. 2017. From Erythroblasts to Mature Red Blood Cells: Organelle Clearance in Mammals. *Front. Physiol.* 8:1076. https://doi.org/10.3389/fphys.2017.01076

Mostowy, S., and P. Cossart. 2012. Septins: the fourth component of the cytoskeleton. *Nat. Rev. Mol. Cell Biol.* 13:183–194. https://doi.org/10.1038/nrm3284

Munjal, A., and T. Lecuit. 2014. Actomyosin networks and tissue morphogenesis. *Development.* 141:1789–1793. https://doi.org/10.1242/dev.091645

Munro, E., J. Nance, and J.R. Priess. 2004. Cortical flows powered by asymmetrical contraction transport PAR proteins to establish and maintain anterior-posterior polarity in the early *C. elegans* embryo. *Dev. Cell.* 7:413–424. https://doi.org/10.1016/j.devcel.2004.08.001

Nguyen, T.Q., H. Sawa, H. Okano, and J.G. White. 2000. The *C. elegans* septin genes, *unc-59* and *unc-61*, are required for normal postembryonic cytokineses and morphogenesis but have no essential function in embryogenesis. *J. Cell Sci.* 113:3825–3837.

Nishimura, H., and S.W. L'Hernault. 2017. Spermatogenesis. *Curr. Biol.* 27:R988–R994. https://doi.org/10.1016/j.cub.2017.07.067

Otomo, T., C. Otomo, D.R. Tomchick, M. Machius, and M.K. Rosen. 2005. Structural basis of Rho GTPase-mediated activation of the formin mDia1. *Mol. Cell.* 18:273–281. https://doi.org/10.1016/j.molcel.2005.04.002

Ovchynnikova, E., F. Aglialoro, M. von Lindern, and E. van den Akker. 2018. The Shape Shifting Story of Reticulocyte Maturation. *Front. Physiol.* 9:829. https://doi.org/10.3389/fphys.2018.00829

Page, B.D., S.J. Diede, J.R. Tenlen, and E.L. Ferguson. 2007. EEL-1, a Hect E3 ubiquitin ligase, controls asymmetry and persistence of the SKN-1 transcription factor in the early *C. elegans* embryo. *Development.* 134:2303–2314. https://doi.org/10.1242/dev.02855

Pavicic-Kaltenbrunner, V., M. Mishima, and M. Glotzer. 2007. Cooperative assembly of CYK-4/MgcRacGAP and ZEN-4/MKLP1 to form the centralspindlin complex. *Mol. Biol. Cell.* 18:4992–5003. https://doi.org/10.1091/mbc.e07-05-0468

Piekny, A.J., and A.S. Maddox. 2010. The myriad roles of Anillin during cytokinesis. *Semin. Cell Dev. Biol.* 21:881–891. https://doi.org/10.1016/j.semcdb.2010.08.002

Praitis, V., E. Casey, D. Collar, and J. Austin. 2001. Creation of low-copy integrated transgenic lines in *Caenorhabditis elegans*. *Genetics.* 157:1217–1226.

Raich, W.B., A.N. Moran, J.H. Rothman, and J. Hardin. 1998. Cytokinesis and midzone microtubule organization in *Caenorhabditis elegans* require the kinesin-like protein ZEN-4. *Mol. Biol. Cell.* 9:2037–2049. https://doi.org/10.1091/mbc.9.8.2037

Rose, L.S., M.L. Lamb, S.N. Hird, and K.J. Kemphues. 1995. Pseudocleavage is dispensable for polarity and development in *C. elegans* embryos. *Dev. Biol.* 168:479–489. https://doi.org/10.1006/dbio.1995.1096

Sallee, M.D., J.C. Zonka, T.D. Skokan, B.C. Raftrey, and J.L. Feldman. 2018. Tissue-specific degradation of essential centrosome components reveals distinct microtubule populations at microtubule organizing centers. *PLoS Biol.* 16:e2005189. https://doi.org/10.1371/journal.pbio.2005189

Sato, K., and M. Sato. 2017. Multiple ways to prevent transmission of paternal mitochondrial DNA for maternal inheritance in animals. *J. Biochem.* 162:247–253.

Sehring, I.M., P. Recho, E. Denker, M. Kourakis, B. Mathiesen, E. Hannezo, B. Dong, and D. Jiang. 2015. Assembly and positioning of actomyosin rings by contractility and planar cell polarity. *eLife.* 4:e09206. https://doi.org/10.7554/eLife.09206

Shirayama, M., M. Seth, H.C. Lee, W. Gu, T. Ishidate, D. Conte Jr., and C.C. Mello. 2012. piRNAs initiate an epigenetic memory of nonself RNA in the *C. elegans* germline. *Cell.* 150:65–77. https://doi.org/10.1016/j.cell.2012.06.015

Srivastava, V., and D.N. Robinson. 2015. Mechanical stress and network structure drive protein dynamics during cytokinesis. *Curr. Biol.* 25:663–670. https://doi.org/10.1016/j.cub.2015.01.025

Strome, S. 1986. Fluorescence visualization of the distribution of microfilaments in gonads and early embryos of the nematode *Caenorhabditis elegans*. *J. Cell Biol.* 103:2241–2252. https://doi.org/10.1083/jcb.103.6.2241

Sulston, J.E., E. Schierenberg, J.G. White, and J.N. Thomson. 1983. The embryonic cell lineage of the nematode *Caenorhabditis elegans*. *Dev. Biol.* 100:64–119. https://doi.org/10.1016/0012-1606(83)90201-4

Tama, F., M. Feig, J. Liu, C.L. Brooks III, and K.A. Taylor. 2005. The requirement for mechanical coupling between head and S2 domains in smooth muscle myosin ATPase regulation and its implications for dimeric motor function. *J. Mol. Biol.* 345:837–854. https://doi.org/10.1016/j.jmb.2004.10.084

Tse, Y.C., M. Werner, K.M. Longhini, J.C. Labbe, B. Goldstein, and M. Glotzer. 2012. RhoA activation during polarization and cytokinesis of the early *Caenorhabditis elegans* embryo is differentially dependent on NOP-1 and CYK-4. *Mol. Biol. Cell.* 23:4020–4031. https://doi.org/10.1091/mbc.e12-04-0268

Watanabe, S., Y. Ando, S. Yasuda, H. Hosoya, N. Watanabe, T. Ishizaki, and S. Narumiya. 2008. mDia2 induces the actin scaffold for the contractile ring and stabilizes its position during cytokinesis in NIH 3T3 cells. *Mol. Biol. Cell.* 19:2328–2338. https://doi.org/10.1091/mbc.e07-10-1086

Zeiser, E., C. Frøkjær-Jensen, E. Jorgensen, and J. Ahringer. 2011. MosSCI and gateway compatible plasmid toolkit for constitutive and inducible expression of transgenes in the *C. elegans* germline. *PLoS One.* 6:e20082. https://doi.org/10.1371/journal.pone.0020082

Zhang, D., and M. Glotzer. 2015. The RhoGAP activity of CYK-4/MgcRacGAP functions non-canonically by promoting RhoA activation during cytokinesis. *eLife.* 4:e08898. https://doi.org/10.7554/eLife.08898

Zonies, S., F. Motegi, Y. Hao, and G. Seydoux. 2010. Symmetry breaking and polarization of the *C. elegans* zygote by the polarity protein PAR-2. *Development.* 137:1669–1677. https://doi.org/10.1242/dev.045823